九州大学学術情報リポジトリ
Kyushu University Institutional Repository

Performance of a hybrid LES/RANS model combined with a wall function for predicting quite high Reynolds-number turbulent channel flows up to Reτ = 6 × 10 7

ABE, Ken-ichi
Department of Aeronautics and Astronautics, Faculty of Engineering, Kyushu University : Professor

https://hdl.handle.net/2324/4151116

出版情報：Journal of Thermal Science and Technology. 15 (12), pp.JTST0014-, 2020. Japan Society of Mechanical Engineers
バージョン：
権利関係：

KYUSHU UNIVERSITY

Bulletin of the JSME

Vol.X, No.X, XXXX

Performance of a hybrid LES/RANS model combined with a wall function for predicting quite high Reynolds-number turbulent channel flows up to $Re_\tau = 6 \times 10^7$

Ken-ichi ABE*

* Department of Aeronautics and Astronautics, Kyushu University
Motooka, Nishi-ku, Fukuoka 819-0395, Japan
E-mail: abe@aero.kyushu-u.ac.jp

Received: X January 2017; Revised: X February 2017; Accepted: X March 2017

Abstract

Performance of an anisotropy-resolving hybrid LES/RANS (HLR) model was investigated. An important feature of this HLR model is the introduction of an extra anisotropic term in a sub-grid scale (SGS) model for large eddy simulation (LES) to represent the SGS stress anisotropy more correctly. Although the basic performance of this model was validated in some previous studies, it is still unclear how the model works for very high Reynolds-number (Re) turbulent flows, in which no-slip wall conditions are no more applicable. Thus, to investigate the predictive performance of this HLR model, it was applied to very high Re turbulent channel flows up to $Re_\tau = 6 \times 10^7$, together with a conventional wall function as the wall-boundary condition. The computational results obtained by the present anisotropic HLR model were carefully compared with those by an isotropic HLR model.

Keywords : Turbulence, Anisotropy-Resolving SGS Model, Hybrid LES/RANS Model, High Reynolds Number, Wall Function

1. Introduction

Large eddy simulation (LES) is known to be a useful way to predict complex turbulence in engineering applications, while there still remains a serious difficulty in its application to very high Reynolds-number (*Re*) flows. To overcome this difficulty, one promising approach is the so-called "hybrid LES/RANS (HLR) model" (see for example, Balaras et al. (1996), Nikitin et al. (2000), Hamba (2001), Davidson and Peng (2003), Piomelli et al. (2003), Batten et al. (2004), Hanjalic et al. (2004), Temmerman et al. (2005), Spalart et al. (2006), Breuer et al. (2008), Deck (2012)). This type of modeling is originally based on the concept of a hybrid model connecting LES with Reynolds-averaged Navier-Stokes (RANS) modeling in the near-wall region.

Recently, an advanced HLR model was proposed by Abe (2014a), in which an anisotropy-resolving sub-grid scale (SGS) model (Abe 2013, Abe 2014b) was adopted in the LES region as well as a one-equation non-linear eddy-viscosity model in the RANS region. An important feature of this SGS model is the introduction of an extra anisotropic term (EAT) to represent the SGS stress anisotropy more correctly. Because most conventional SGS models generally include only the eddy-viscosity term, they can never represent the SGS stress anisotropy. In contrast, the present SGS model introduces an EAT based on the concept of the scale-similarity model (Bardina et al. (1980)), providing more proper SGS stress anisotropy. Although the basic performance of this model was validated by its application to several wall-shear flows and some separated flows under various grid-resolution conditions (Abe 2014a), it is still unclear how the model works for very high *Re* turbulent flows.

On the other hand, another crucial concern of the HLR modeling strategy is the so-called "double-buffer problem" that is often seen in the mean-velocity prediction. In fact, many HLR models are likely to show unphysical mean-velocity distributions in the LES/RANS interface region, where steeper mean-velocity gradients are seen. Surprisingly, however, the aforementioned anisotropy-resolving HLR model (Abe 2014a) did not show or, at least, largely reduced the "double-buffer problem" in the mean-velocity distribution, although no other special treatment was applied in the LES/RANS

interface region. To explain why this HLR model can reduce the "double-buffer problem" in the LES/RANS interface region, Abe (2018) investigated the model performance at various grid resolutions by applying the model to a plane channel flow at $Re_\tau = 1 \times 10^3$. It was found that the vortex structures were divided into smaller sizes as an effect of the EAT, resulting in a successful improvement of the "double-buffer problem." Although the feature obtained from previous studies are encouraging for developing HLR models, it should be important to confirm the predictive performance of the model for very higher Re turbulent flows, in which no-slip wall conditions are no more applicable.

The main purpose of the present study is to investigate the predictive performance of this anisotropy-resolving HLR model for very high Re turbulent channel flows up to $Re_\tau = 6 \times 10^7$, where Re_τ is the Reynolds number based on the friction velocity. We focus specifically on the role of the EAT introduced in the SGS model for such high Re flows. The computational results obtained by the present anisotropic HLR model are carefully compared with those by an isotropic HLR model without the EAT.

2. Governing Equations and Turbulence Model

The filtered (or Reynolds-averaged) governing equations for an incompressible turbulent flow are expressed as follows:

$$\frac{\partial \overline{U}_i}{\partial x_i} = 0, \tag{1}$$

$$\frac{\mathrm{D}\overline{U}_i}{\mathrm{D}t} = -\frac{1}{\rho}\frac{\partial \overline{P}}{\partial x_i} + \frac{\partial}{\partial x_j}\left\{\nu\left(\frac{\partial \overline{U}_i}{\partial x_j} + \frac{\partial \overline{U}_j}{\partial x_i}\right) - \tau_{ij}\right\}, \tag{2}$$

where $\overline{(\ )}$ denotes a filtered value in the LES region or a Reynolds-averaged value in the RANS region, respectively. In Eqs. (1) and (2), ρ, $\overline{P}$ and $\overline{U}_i$ denote the density, filtered static pressure and filtered velocity, respectively.

Originally, the HLR model is a turbulence model that uses LES in the region far from the wall, while RANS is adopted in the near-wall region. To connect these LES and RANS regions smoothly, the following hybrid approach is adopted:

$$\phi = (1 - f_{hb})\ \phi_{(RANS)} + f_{hb}\ \phi_{(LES)}, \tag{3}$$

where ϕ is a flow variable and f_{hb} is a switching function. In Eq. (3), f_{hb} is close to 1 in the region far from the wall, where LES is adopted. Conversely, as f_{hb} approaches 0, the RANS calculation is adopted. For instance, if we consider the SGS (Reynolds) stress τ_{ij}, the expression is written as

$$\tau_{ij} = (1 - f_{hb})\ \tau_{ij(RANS)} + f_{hb}\ \tau_{ij(LES)}. \tag{4}$$

Here, we briefly describe the SGS stress $\tau_{ij(LES)}$ in Eq. (4), that is modeled as

$$\tau_{ij(LES)} = \frac{2}{3}\, k_{SGS}\ \delta_{ij} - 2\ \nu_{SGS}\ S_{ij} + 2\ k_{SGS}\ b_{ij}^{EAT}, \tag{5}$$

where k_{SGS}, ν_{SGS} and S_{ij} are the SGS turbulence energy, the SGS eddy viscosity and the strain-rate tensor, respectively. The third term on the right-hand side in Eq. (5) is regarded as the EAT, in which the anisotropy tensor b_{ij}^{EAT} is modeled as

$$b_{ij}^{EAT} = \frac{\tau'_{ij} - \left(-2\nu' S_{ij}\right)}{\tau'_{kk} - (-2\nu' S_{kk})} - \frac{1}{3}\delta_{ij} = \frac{R'_{ij}}{\tau'_{kk}}, \qquad R'_{ij} = \tau'^{\,a}_{ij} - \left(-2\nu' S_{ij}\right), \tag{6}$$

where $\tau'^{\,a}_{ij} = \tau'_{ij} - \tau'_{kk}\delta_{ij}/3$. In Eq. (6), τ'_{ij} is given by the following representative scale-similarity model of Bardina et al. (1980):

$$\tau'_{ij} = \left(\overline{U}_i - \widehat{\overline{U}}_i\right)\left(\overline{U}_j - \widehat{\overline{U}}_j\right), \tag{7}$$

where $\widehat{(\ )}$ denotes a test-filtered value. In the model, ν' is an equivalent eddy viscosity evaluated using an isotropic EVM-type (EVM: eddy-viscosity model) linear approximation for Eq. (7),

$$\tau'^{\,a}_{ij} S_{ij} = -2\nu' S_{ij} S_{ij} = -2\nu' S^2 \quad \longrightarrow \quad \nu' = -\frac{\tau'^{\,a}_{ij} S_{ij}}{2S^2}, \tag{8}$$

where $S^2 = S_{ij}S_{ij}$. As R'_{ij} in Eq. (6) is evaluated by subtracting an isotropic EVM form from the original Bardina et al. (1980) model, the EAT in Eq. (5) including R'_{ij} is then expected to successfully predict the SGS-stress anisotropy (Ohtsuka and Abe (2014)).

Concerning the linear EVM in Eq. (5), we basically adopts the one-equation SGS model proposed by Inagaki (2011) with some minor modifications. More detailed descriptions of the present anisotropy-resolving SGS model are given in Abe (2013) and Abe (2014b). Furthermore, detailed descriptions of the one-equation non-linear eddy-viscosity model for $\tau_{ij(RANS)}$ and the switching function f_{hb} are given in Abe (2014a) and Abe (2018).

Next, we decompose the modeled stresses into isotropic and anisotropic parts to make discussion point clearer. In general, the canonical form of the SGS stress is expressed as

$$\tau_{ij(LES)} = \frac{2}{3}k_{SGS}\delta_{ij} - 2\,\nu_{SGS}S_{ij} + EAT_{ij} = EVM_{ij(LES)} + EAT_{ij}, \tag{9}$$

where EAT_{ij} is the anisotropic part of the SGS stress that is the same as the EAT in this study. Note that for RANS, we often use the following expression for the Reynolds stress:

$$\tau_{ij(RANS)} = \frac{2}{3}k\delta_{ij} - 2\,\nu_t S_{ij} + HOT_{ij} = EVM_{ij(RANS)} + HOT_{ij}, \tag{10}$$

where k and ν_t are the turbulence energy and the eddy viscosity, respectively. In Eq. (10), HOT_{ij} is a kind of EAT but is usually called the higher-order term (HOT) because this term consists of second- and/or third-order products of the strain-rate and vorticity tensors. As mentioned before, this kind of RANS model is generally called "non-linear eddy-viscosity model." Because conventional linear EVMs generally include only the eddy-viscosity term, they can never represent the Reynolds-stress anisotropy. In this sense, HOT is regarded as a term to represent the Reynolds-stress anisotropy more correctly.

If we connect the LES and RANS regions according to Eq. (4), τ_{ij} is written as

$$\begin{aligned}\tau_{ij} &= (1 - f_{hb})\ \tau_{ij(RANS)} + f_{hb}\ \tau_{ij(LES)} \\ &= (1 - f_{hb})\ EVM_{ij(RANS)} + f_{hb}\ EVM_{ij(LES)} + \left[(1 - f_{hb})\ HOT_{ij} + f_{hb}\ EAT_{ij}\right].\end{aligned} \tag{11}$$

Finally, we obtain

$$\tau_{ij} = (1 - f_{hb})\ EVM_{ij(RANS)} + f_{hb}\ EVM_{ij(LES)} + EAT_{ij(HLR)}, \tag{12}$$

where

$$EAT_{ij(HLR)} = (1 - f_{hb})\ HOT_{ij} + f_{hb}\ EAT_{ij}. \tag{13}$$

If we take only the first two terms on the right-hand side of Eq. (12), τ_{ij} has a canonical form of isotropic EVM that is generally used for other HLR models.

By substituting Eq. (12) into Eq. (2), the divergence of the EAT

$$-\frac{\partial EAT_{ij(HLR)}}{\partial x_j} \tag{14}$$

can be regarded as an additional source term in the transport equation that directly influences the momentum in the i-direction. It is noted that the effect of Eq. (14) originally derives from a physics-oriented discussion because the EAT_{ij} in Eq. (13) is based on the scale-similarity modeling concept (Bardina et al. 1980).

3. Test Cases and Computational Conditions

The primary concern of this study is to investigate the predictive performance of the anisotropy-resolving HLR model for high Re turbulent flows. To investigate this issue, we apply two types of HLR models to fully-developed plane channel flows at several Reynolds numbers up to $Re_\tau = 6 \times 10^7$. One of the models is the original (full) version of the anisotropic HLR model as described in Eq. (12), and the other is its isotropic EVM version consisting of only the first two terms on the right-hand side of Eq. (12). In this study, the former full version is referred to as "HLR-EAT," while the latter as "HLR-NOEAT."

Table 1 Computational parameters for channel-flow cases.

Case	Grid numbers	Domain(x-y-z)	Δx	Δy	Δz
C1E6	257×181×257	$6.4\delta \times 2\delta \times 3.2\delta$	0.025	3×10^{-4} –0.034	0.013
C1E7	257×181×257	$6.4\delta \times 2\delta \times 3.2\delta$	0.025	3×10^{-5} –0.049	0.013
C6E7	257×181×257	$6.4\delta \times 2\delta \times 3.2\delta$	0.025	5×10^{-6} –0.06	0.013

Case	Re_τ	Δx^+	Δy^+	Δz^+	Δt
C1E6	1×10^6	2.5×10^4	300–3.4×10^4	1.3×10^4	1.5×10^{-4}
C1E7	1×10^7	2.5×10^5	300–4.9×10^5	1.3×10^5	1×10^{-4}
C6E7	6×10^7	1.5×10^6	300–3.6×10^6	7.5×10^5	2×10^{-5}

The computational conditions are summarized in Table 1. In this study, the computational domain was fixed to be $6.4\delta \times 2\delta \times 3.2\delta$ in the streamwise (x), wall-normal (y) and spanwise (z) directions, respectively, where δ is the half channel height. The number of grid nodes was also fixed, consisting of 257×181×257 in x, y and z directions, respectively, although the grid spacing in the wall-normal (y) direction was changed according to the Reynolds number.

In this study, we tried to calculate flow fields for extremely high *Re* conditions. Particularly, for the highest *Re* case C6E7, the bulk Reynolds number becomes around 5×10^9 and then the grid resolutions in the streamwise and spanwise directions are too coarse for resolving the near-wall vortex structures, as shown in Table 1. Furthermore, the grid resolution in the wall-normal direction is also very coarse in this study, where no-slip wall conditions are no more applicable. Therefore, the present conditions are expected to be very severe for HLR models.

In this study, the computational procedure used is the same as that of Abe (2018). This is an unstructured finite-volume procedure nearly identical to that of Muto et al. (2012), where a vertex-centered type of storage is used on a grid. We generally adopt the second-order central difference scheme to discretize the spatial derivatives. Note that the convection terms of the momentum equations are discretized by a blending scheme of the second-order central difference (98%) and the first-order upwind scheme (2%) so as to eliminate unnecessary numerical instability that may appear when we use very high aspect ratio of the grid spacing in the near-wall region for high *Re* turbulent flows. It is also noted that the convection term of the turbulence energy is discretized by the second-order upwind scheme. The time marching is based on the fractional step method (Kim and Moin 1985), in which the second-order Crank-Nicolson scheme is used for the velocity equations. Note that the first-order Euler implicit scheme is used for the transport equation of the turbulence energy. The coupling of the velocity and pressure fields is based on the simplified marker and cell method (Amsden and Harlow 1970). The flow rate on the control-volume surface is estimated using the Rhie-Chow interpolation (Rhie and Chow 1983). In our previous studies, we carefully investigated the effects of the blending scheme used for the momentum equation (Abe 2018), as well as the first-order time-marching scheme and the second-order upwind scheme adopted for the transport equation of turbulence energy (Abe 2013, Abe 2014b). These investigations confirmed that the time-integration and space-discretization schemes used in these transport equations did not have any crucial effect on the final conclusions.

For the boundary conditions, the periodic condition is imposed in the streamwise and spanwise directions. Concerning the wall-normal direction, the grid node next to the wall surface is located at $y^+ = 300$, which is too far to specify the no-slip conditions. Therefore, a conventional wall function is adopted for the wall-boundary condition.

4. Results and Discussion

4.1. Basic performance of the present HLR model with wall function

First, to discuss the basic performance of the HLR models with wall function being used as the wall boundary condition, the mean-velocity distributions are compared in Fig. 1. Note that the distributions of the switching function f_{hb} are also shown. As seen in Fig. 1 (a), the present anisotropic HLR model (HLR-EAT) provides generally reasonable predictions that agree well with the logarithmic-low distribution. More importantly, the "double-buffer problem" is not seen in the mean-velocity distributions, at least, for these three test cases. In contrast, from Fig. 1 (b), the predictions obtained using the isotropic EVM (HLR-NOEAT) clearly show the "double-buffer problem" in the LES/RANS interface region, where steeper mean-velocity gradients are seen for all cases. As these two HLR models adopt the same form of EVM part, this difference in the mean-velocity predictions is thought to be caused by the EAT that has been introduced in Eq. (12). Considering the fact that the results are obtained using a conventional wall function, it is also understood that this improvement for the "double-buffer problem" does not derive from the low *Re*-number model functions involved in the present HLR model (Abe 2014a).

Figure 2 compares the distributions of the total *Re*-shear stress and turbulence energy predicted by the HLR-EAT and the HLR-NOEAT. Note that the distributions include the contribution of the modeled (SGS) part as well as the resolved

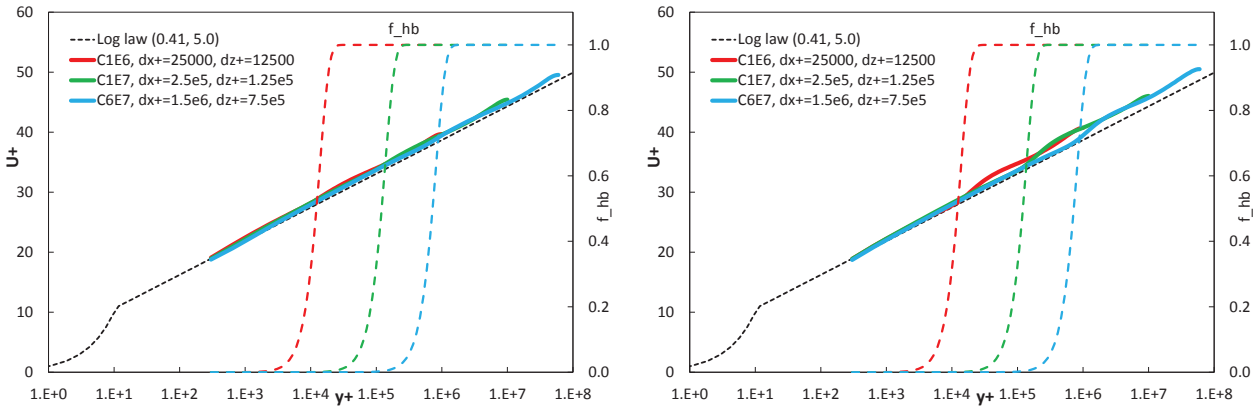

(a) The present model (HLR-EAT) (b) Isotropic model (HLR-NOEAT)

Fig. 1 Comparison of the mean-velocity distributions for various Reynolds numbers up to $Re_\tau = 6 \times 10^7$.

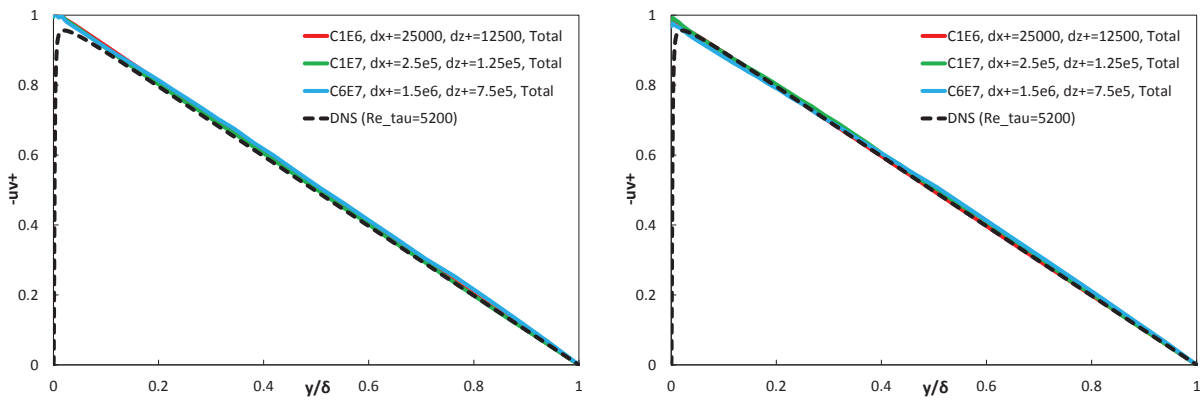

(a) HLR-EAT (b) HLR-NOEAT

Total (GS+SGS) Reynolds-shear stress

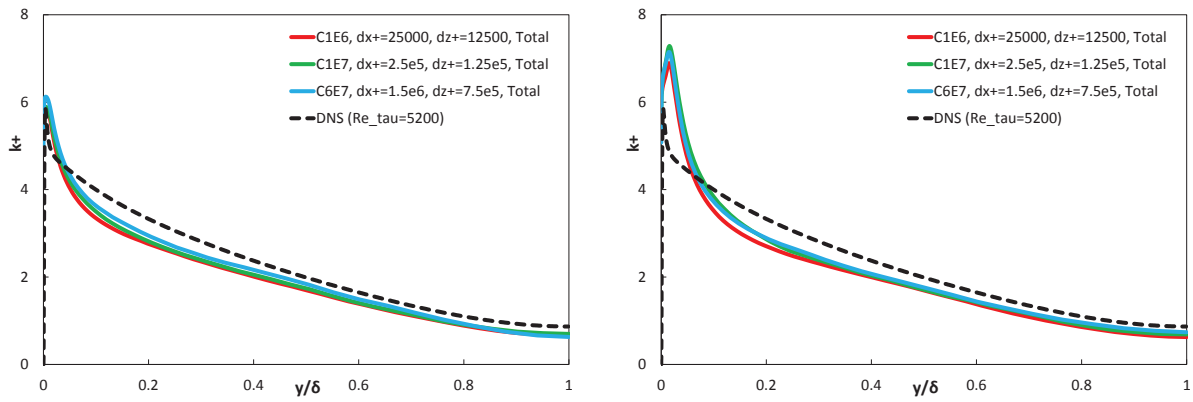

(c) HLR-EAT (d) HLR-NOEAT

Total (GS+SGS) turbulence energy

Fig. 2 Comparison of the *Re*-shear stress and the turbulence energy for various Reynolds numbers up to $Re_\tau = 6 \times 10^7$.

(grid-scale: GS) part. In the figure, the DNS data at $Re_\tau = 5200$ provided by Lee and Moser (2015) are also included for reference because this is considered to be one of the highest *Re* conditions among available DNS data.

As seen in Fig. 2 (a), the *Re*-shear stress predicted by the HLR-EAT shows reasonable trend that is in no conflict with the DNS data. As for turbulence energy in Fig. 2 (c), the HLR-EAT also provides reasonable predictions in general, although a detailed investigation indicates that the predictions show some overpredictions in the near-wall region as well as some underpredictions in the region far from the wall, compared with the DNS data. On the other hand, it is found from Fig. 2 (d) that the HLR-NOEAT returns poorer predictions for the turbulence energy as considerable overpredictions

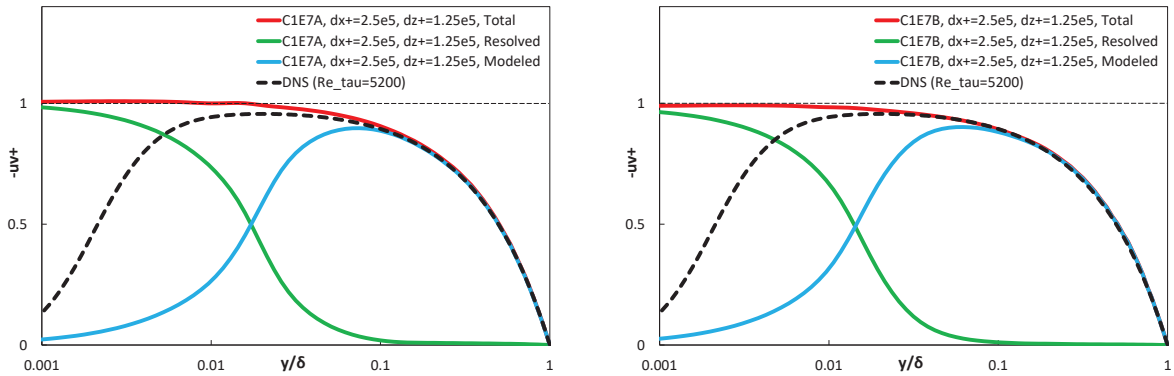

(a) HLR-EAT (b) HLR-NOEAT

GS, SGS and Total (GS+SGS) Reynolds-shear stress

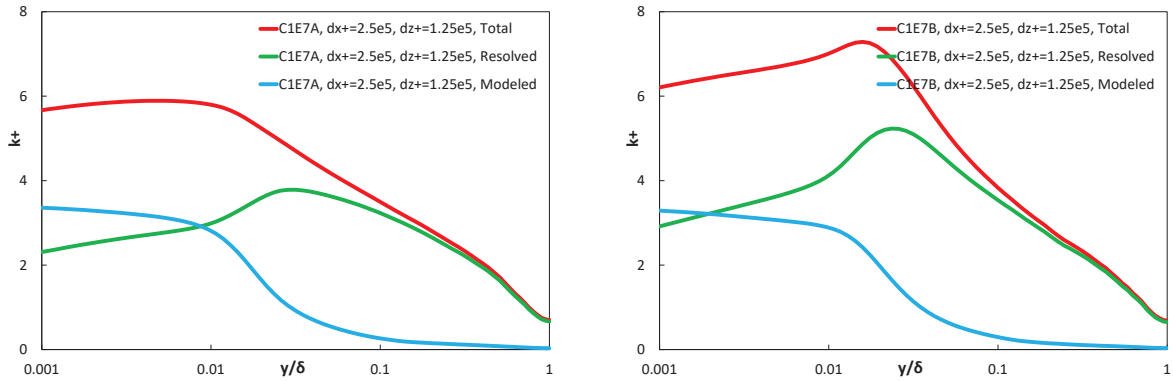

(c) HLR-EAT (d) HLR-NOEAT

GS, SGS and Total (GS+SGS) turbulence energy

Fig. 3 Comparison of the *Re*-shear stress and the turbulence energy at $Re_\tau = 1 \times 10^7$ (log scale for horizontal axis).

are seen in a wider range of the near-wall region. In regard to the *Re*-shear stress predicted by the HLR-NOEAT in Fig. 2 (b), the distributions seem to be generally reasonable. This indicates that only a slight difference in the *Re*-shear stress in the LES/RANS interface region may cause the "double-buffer problem" that is seen in Fig. 1.

Figure 3 compares the resolved and modeled components of the *Re*-shear stress and turbulence energy at $Re_\tau = 1 \times 10^7$, as well as their total values. To discuss the distributions in the LES/RANS interface region in more detail, the horizontal axis in this figure is plotted in log scale. As for the *Re*-shear stress, the careful investigation indicates that the HLR-NOEAT shows slightly lower values at around $y/\delta = 0.02$ compared with those by the HLR-EAT. This underestimation is considered to be related to the difference in the mean-velocity prediction. However, the difference is not always remarkable, and thus further detailed investigation is necessary in future work.

Concerning the turbulence energy, we can clearly see differences in the results between two models. It is interesting that the difference is particularly recognized in the resolved part of the HLR-NOEAT results. A typical feature is that unnatural peaks appear at around the LES/RANS interface location in Fig. 3 (d) . Because a similar trend was also found in our previous study (Abe 2018) for a lower *Re* case ($Re_\tau = 1000$), the insight obtained here is thought to be an essential feature of the HLR-NOEAT.

4.2. Effect of the EAT on turbulent structures in the LES/RANS interface region

As discussed in the above section, we can see considerable differences in the predictions between the HLR-EAT and the HLR-NOEAT. As for this issue, it is useful to investigate the unsteady flow structures in the LES/RANS interface region, where most differences appear. First, to confirm the location of the interface region, the distributions of the switching function f_{hb} is shown in Fig. 4, where it is plotted in wall units and in global range, respectively. The switching function f_{hb} in the present HLR model is basically composed of the local grid spacing and the wall distance (Abe 2014a). Although we can see large differences in the distributions in Fig. 4 (a) shown in wall units, the distributions in Fig. 4 (b)

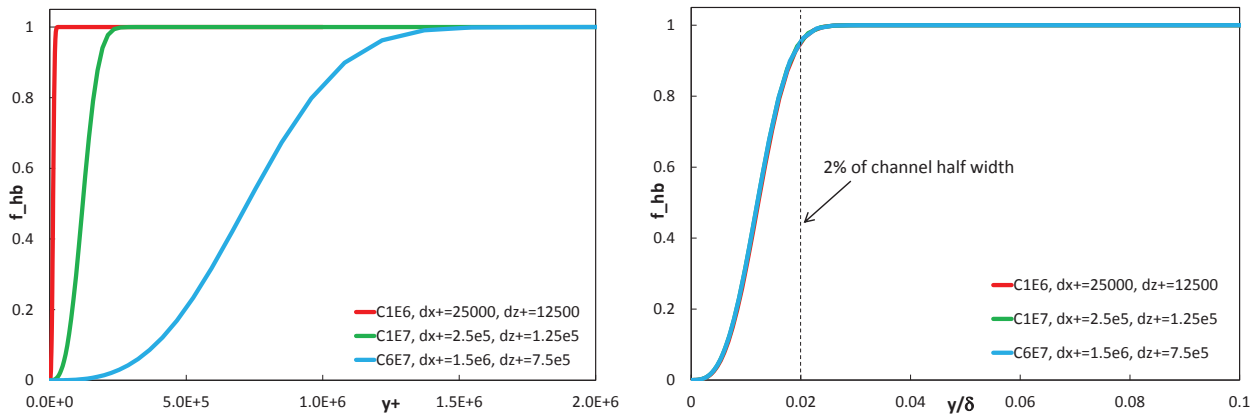

(a) Distributions in wall units (b) Distributions in global range

Fig. 4 Comparison of the distributions of the switching function f_{hb} (HLR-EAT).

shown in global range are basically identical for all test cases. For instance, as seen in Fig. 4 (a), f_{hb} begins to change from 1 (LES) to 0 (RANS) at around $y^+ \sim 1\times10^6$ for the highest Re case at $Re_\tau = 6\times10^7$. However, this y location is just about 2% of the half channel height (i.e., $\delta^+ = 6\times10^7$) and thus most of the computational domain is covered by LES in the present simulations (Fig. 4 (b)). To investigate the effect of the EAT on the unsteady turbulent structures, it should be important to compare the results between the HLR-EAT and the HLR-NOEAT in the LES/RANS interface region, where f_{hb} begins to change from 1 to 0.

For this purpose, Fig. 5 compares the distributions of the instantaneous streamwise velocity fluctuation at $y/\delta = 0.02$ and $y/\delta = 1$ for C6E7. Note that as seen in Fig. 4 (b), the location of $y/\delta = 0.02$ is at around the edge of the LES/RANS interface region. On the other hand, the far-field location of $y/\delta = 1$ is selected for comparison because it is always involved in the LES region ($f_{hb} = 1$). As found from Fig. 5 (a) and (b) at $y/\delta = 0.02$, the results by the HLR-EAT show small-scale turbulent structures, while the sizes of the structures provided by the HLR-NOEAT look larger at this location. This fact can be confirmed more clearly by comparing Fig. 5 (c) and (d) that are zoomed from Fig. 5 (a) and (b), respectively. This is considered to be closely related to the improvement of the mean-velocity distribution as seen in Fig. 1 (a). On the other hand, looking at Fig. 5 (e) and (f), both the HLR-EAT and the HLR-NOEAT show a similar trend at $y/\delta = 1$, where small-scale fluctuations tend to decrease, whereas large-scale flow patterns are mainly seen at the far-field location.

To investigate the size of the vortex structures in more detail, Fig. 6 compares the energy spectrum of the streamwise velocity fluctuation for the highest Re case (C6E7) at $Re_\tau = 6\times10^7$. Note that two y locations in the figure are identical to those discussed in Fig. 5: the location of $y/\delta = 0.02$ is in the LES/RANS interface region and $y/\delta = 1$ (i.e., the channel center) is in the LES region. First, from Fig. 6 (a) at $y/\delta = 0.02$, we can understand a definite difference in the energy spectrum between the HLR-EAT and the HLR-NOEAT. The distribution of the HLR-EAT provides considerably higher values of the spectrum compared with that of the HLR-NOEAT, particularly in the high wave-number region. This fact sufficiently supports the insight obtained from the comparison between Fig. 5 (a) and (b) that the HLR-EAT generates smaller-scale turbulent structures in the LES/RANS interface region. In contrast, as seen in Fig. 6 (b) at the far-field location of $y/\delta = 1$, almost the same spectrum distributions are obtained for both two models.

In our previous study (Abe 2018), we investigated the influence of the EAT on the vortex structures for a lower Re case ($Re_\tau = 1000$) using relatively coarse grid resolutions. The distributions of the velocity fluctuations in Abe (2018) showed trends similar to those in the present study. Turbulent structures in the HLR-EAT results at around the LES/RANS interface location looked smaller than those of the HLR-NOEAT. It was also confirmed by the correlation coefficient in the spanwise direction that the scales of vortex structures in the HLR-EAT results were generally smaller than those in the HLR-NOEAT results at around the LES/RANS interface location (Abe 2018). Such being the case, these trends are seen in both our previous (Abe 2018) and the present studies, and thus the influence of the EAT in the LES/RANS interface region is thought to be a common feature of this kind of HLR models, regardless of the flow Reynolds number.

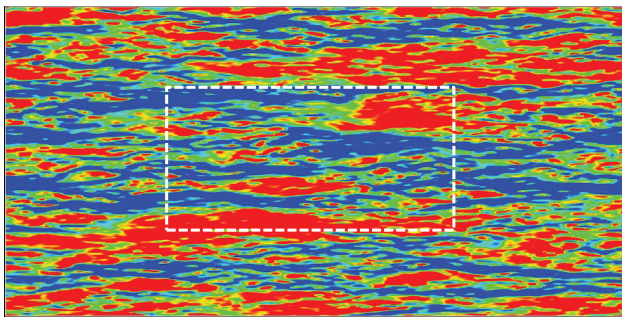

(a) HLR-EAT

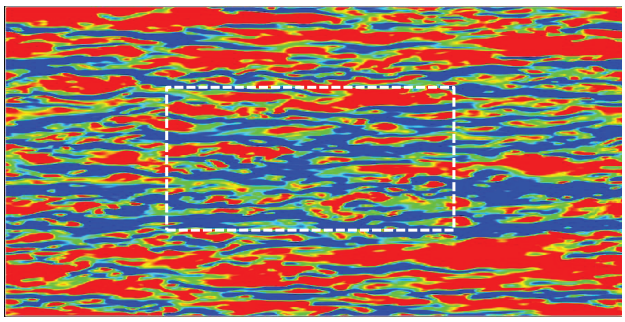

(b) HLR-NOEAT

LES/RANS interface region ($y/\delta = 0.02$)

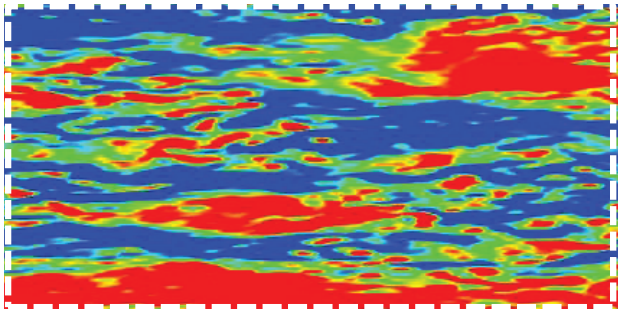

(c) HLR-EAT

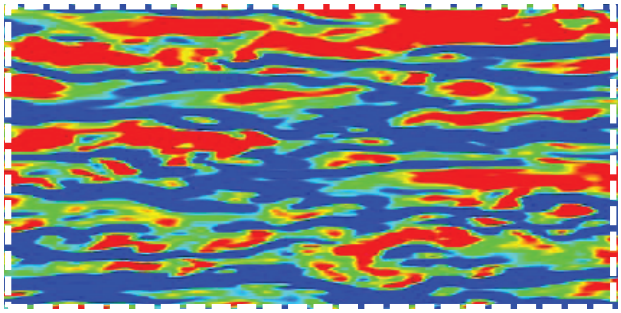

(d) HLR-NOEAT

LES/RANS interface region ($y/\delta = 0.02$), zoomed in (white broken-line box)

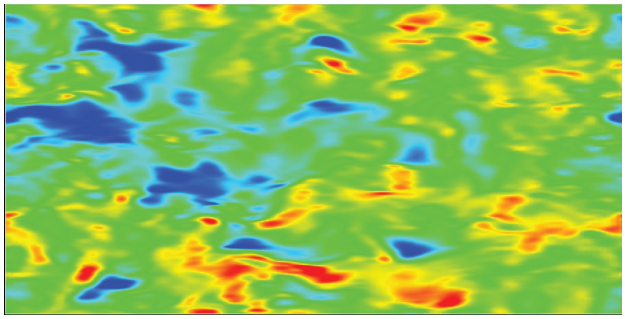

(e) HLR-EAT

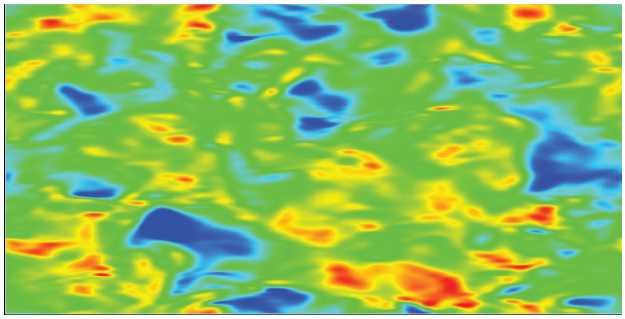

(f) HLR-NOEAT

LES region ($y/\delta = 1$)

Fig. 5 Comparison of the streamwise velocity fluctuation at $Re_\tau = 6\times10^7$ (color ranges from −2 (blue) to 2 (red), normalized in wall units).

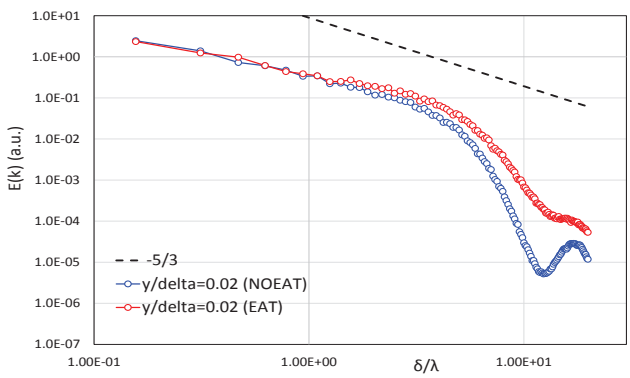

(a) LES/RANS interface region ($y/\delta = 0.02$)

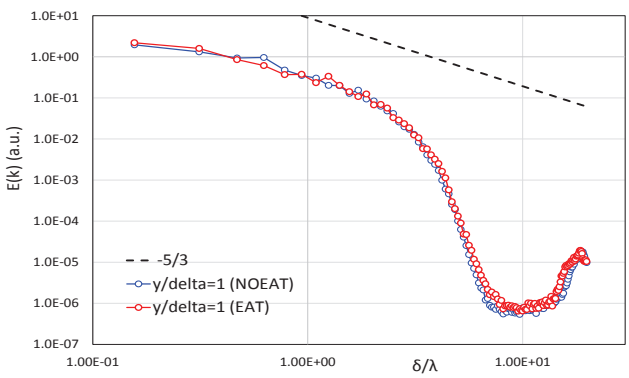

(b) LES region ($y/\delta = 1$)

Fig. 6 Comparison of the energy spectrum of the streamwise velocity fluctuation at $Re_\tau = 6\times10^7$.

5. Concluding Remarks

To investigate the predictive performance of an anisotropy-resolving hybrid LES/RANS (HLR) model for very high *Re* turbulent flows, in which no-slip wall conditions are no more applicable, we applied the model to fully-developed plane channel flows at several Reynolds numbers up to $Re_\tau = 6 \times 10^7$ with a conventional wall function as the wall-boundary condition. We focused specifically on the role of the extra anisotropic term (EAT) introduced in the SGS model for such high *Re* turbulent flows. For this purpose, the computational results obtained by the present model (HLR-EAT) were carefully compared with those by an isotropic HLR model without the EAT (HLR-NOEAT).

Concerning the distributions of the mean values, the HLR-EAT provided generally reasonable predictions. In contrast, the HLR-NOEAT clearly showed the "double-buffer problem" in the LES/RANS interface region, where steeper mean-velocity gradient was seen. Furthermore, we compared the results for instantaneous velocity fluctuations obtained with and without the EAT. The comparison indicated that the vortex structures were found to be divided into smaller sizes as an effect of the EAT. In addition, we calculated the energy spectrum of the velocity fluctuations to investigate how the structure sizes distributed in the wave-number space. We found that the EAT had a potential to increase the energy spectrum in the LES/RANS interface region, particularly in the high wave-number space. This is a notable feature of the present HLR model.

From these investigations, it is found that the EAT introduced in the SGS model largely affects the enhancement of vortex structures in the LES/RANS interface region. This feature is considered to work for improving the mean-velocity distribution with no (or, at least, very small) "double-buffer problem." These findings indicate a high potential of the present anisotropy-resolving HLR model even for very high *Re* turbulent flows.

Acknowledgements

The present computation was primarily carried out using the computer facilities at the Research Institute for Information Technology, Kyushu University, Japan. This research was supported by JSPS KAKENHI Grant Number JP19K12005. The present images were partially created using FieldView as provided by Intelligent Light through its University Partners Program.

References

Abe, K., An improved anisotropy-resolving subgrid-scale model with the aid of a scale-similarity modeling concept, International Journal of Heat and Fluid Flow, Vol.39(2013), pp.42-52.

Abe, K., An advanced switching parameter for a hybrid LES/RANS model considering the characteristics of near-wall turbulent length scales, Theoretical and Computational Fluid Dynamics, Vol.28(2014a), pp.499-519, DOI: 10.1007/s00162-014-0328-3.

Abe, K., An investigation of SGS-stress anisotropy modeling in complex turbulent flow fields, Flow, Turbulence and Combustion, Vol.92(2014b), pp.503-525.

Abe, K., Improvement of double-buffer problem in LES-RANS interface region by introducing an anisotropy-resolving subgrid-scale model, Theoretical and Computational Fluid Dynamics, Vol.32(2018), pp.263-283, DOI: 10.1007/s00162-018-0453-5.

Amsden, A.A., and Harlow, F.H., A simplified MAC technique for incompressible fluid flow calculations. Journal of Computational Physics, Vol.6(1970), pp.322-325.

Balaras, E., Benocci, C., and Piomelli, U., Two-layer approximate boundary conditions for large-eddy simulations. AIAA Journal, Vol.34(1996), pp.1111-1119.

Batten, P., Goldberg, U., and Chakravarthy, S., Interfacing statistical turbulence closures with large-eddy simulation. AIAA Journal, Vol.42(2004), pp.485-492.

Bardina, J., Ferziger, J.H., and Reynolds, W.C., Improved subgrid scale models for large eddy simulation, AIAA Paper, No. 80-1357(1980).

Breuer, M., Jaffrezic, B., and Arora, K., Hybrid LES/RANS technique based on a one-equation near-wall model, Theoretical and Computational Fluid Dynamics, Vol.22(2008), pp.157-187.

Davidson, L., and Peng, S.H., Hybrid LES-RANS modelling: a one-equation SGS model combined with a k-ω model for predicting recirculating flows. International Journal of Numerical Methods for Fluids, Vol.43(2003), pp.1003-1018.

Deck, S., Recent improvements in the Zonal Detached Eddy Simulation (ZDES) formulation. Theoretical and Computational Fluid Dynamics, Vol.26(2012), pp.523-550.

Hamba, F., An attempt to combine large eddy simulation with the k-ε model in a channel-flow calculation. Theoretical and Computational Fluid Dynamics, Vol.14(2001), pp.323-336.

Hanjalic, K, Hadziabdic, M., Temmerman, L., and Leschziner, M.A., Merging LES and RANS strategies: zonal or seamless coupling? Direct and Large Eddy Simulation V (R. Friedrich et al. (eds)), Kluwer Academic Publishers(2004), pp.451-464.

Inagaki, M., A new wall-damping function for large eddy simulation employing Kolmogorov velocity scale, International Journal of Heat and Fluid Flow, Vol.32(2011), pp.26-40.

Kim, J., and Moin, P., Application of a fractional-step method to incompressible Navier-Stokes equations. Journal of Computational Physics, Vol.59(1985), pp.308-323.

Lee, M., and Moser, R. D., Direct numerical simulation of turbulent channel flow up to Re_τ = 5200, Journal of Fluid Mechanics, Vol.774(2015), pp.395-415.

Muto, M., Tsubokura, M., and Oshima, N., Negative Magnus lift on a rotating sphere at around the critical Reynolds number, Physics of Fluids, Vol.24(2012), No. 014102.

Nikitin, N.V., Nicoud, F., Wasistho, B., Squires, K.D., and Spalart, P.R., An approach to wall modeling in large-eddy simulations. Physics of Fluids, Vol.12(2000), pp.1629-1632.

Ohtsuka, T., and Abe, K., Toward the development of an anisotropy-resolving subgrid-scale model for large eddy simulation. Journal of Fluid Science and Technology, Vol.9(2014), JFST0004, DOI:10.1299/jfst.2014jfst0004.

Piomelli, U., Balaras, E., Pasinato, H., Squaires, K.D., and Spalart, P.R., The inner-outer layer interface in large-eddy simulations with wall-layer models. International Journal of Heat and Fluid Flow, Vol.24(2003), pp.538-550.

Rhie, C.M., and Chow, W.L., Numerical study of the turbulent flow past an airfoil with trailing edge separation. AIAA Journal, Vol.21(1983), pp.1525-1532.

Spalart, P.R., Deck, S., Shur, M.L., Squires, K.D., Strelets, M.Kh., and Travin, A., A new version of detached-eddy simulation, resistant to ambiguous grid densities. Theoretical and Computational Fluid Dynamics, Vol.20(2006), pp.181-195.

Temmerman, L., Hadziabdic, M., Leschziner, M.A., and Hanjalic, K., A hybrid two-layer URANS-LES approach for large eddy simulation at high Reynolds numbers. International Journal of Heat and Fluid Flow, Vol.26(2005), pp.173-190.